ISBN: 978-3-95450-214-1 ISSN: 2673-5490 doi:10.18429/JACoW-IPAC2021-MOPAB044

GAS BREMSSTRAHLUNG MEASUREMENTS IN THE ADVANCED PHOTON SOURCE STORAGE RING*

J. Dooling†, A. Brill, J. Calvey
Argonne National Laboratory, 9700 S. Cass Ave., Lemont, IL 60439, USA

Abstract

In the Advanced Photon Source Upgrade storage ring (SR), small-aperture vacuum chambers provide limited conductance for pumping. Non-evaporable getter coatings will be used in the SR to support the vacuum. Ion pumps and cold- cathode gauges are typically located away from the vacuum chamber transporting the beam. Measuring gas bremsstrahlung (GB) photons in low-conductance chambers provides a method to determine the pressure at the beam location. We report on GB measurements made in the ID-25 beamline. A Pb:Glass calorimeter radiator generates Čerenkov radiation when high-energy photons cause pair-production within the glass. A photomultiplier tube converts the light pulses to electrical signals. Data sets were obtained during normal machine operations starting in January 2020. Data collection was facilitated using a 4-channel ITech Beam Loss Monitor FPGA that allows for control of thresholds and attenuation settings in both counting and pulse-height acquisition modes. Count rates and spectra were recorded for the three primary fill patterns typically used during SR operations as well as during gas injection experiments; results of these measurements will be presented.

INTRODUCTION

The Sector 25 Insertion Device (25ID) beam line was one of the last to be built out at the Advanced Photon Source (APS). Prior to beam line construction starting in August 2020, the 25ID undulator straight section was used for several experiments concluding with a gas injection ion instability study [1, 2]. A gas bremsstrahlung (GB) detector was installed downstream of the gas injection location to record this high-energy photon radiation during the ion instability experiments as well as normal operations.

For a thin target, the radiative energy loss from a mono-energetic electron beam may be written as [3]

$$\left.\frac{dW}{dz}\right|_{rad} = -\frac{\rho W}{X_o}, \qquad (1)$$

where W is the electron kinetic energy, ρ is the density of the target, and X_o is the radiation length. This leads to the simple solution, $W(z) = W_o \exp(-\rho z/X_o)$ where W_o is the initial kinetic energy. At high energy ($W \gg m_o c^2$), radiative loss dominates. Radiative loss from the electron beam is the source of GB photons. At standard temperature and pressure (1 atm) the density of air is 0.0012 g/cm^3. The radiation length in dry air is 36.6 g/cm^2 [4]; in units of distance, $t = X_o/\rho = 3.04 \times 10^4$ cm. Thus even with a pressure of 1000 nTorr, $\rho L_{ss}/X_o \ll 1$ where the long straight section distance, $L_{ss} = 1538$ cm. The average energy lost per electron in length z (or gained by the GB radiation) is $W_o \rho z/X_o$.

GB radiation striking a Pb:Glass target was simulated with MARS [5]; the geometry is presented in Fig. 1. A 24-cm

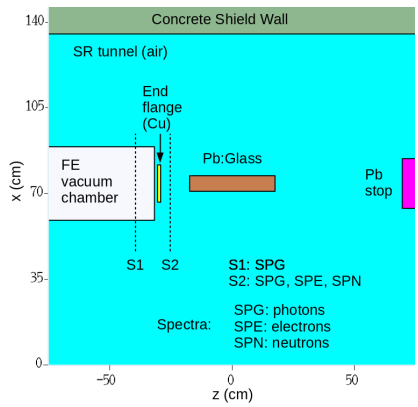

Figure 1: MARS geometry in plan view at beam elevation. Spectra were recorded at locations S1 and S2.

length air target at 760 Torr was used to generate the photon flux; whereas, the corrected target assumes 1000 nTorr of N_2 over a length of 500 cm. The scale factor then is 2.74×10^{-8}; for normal operations at 1 nTorr, the scale factor is approximately 3 orders of magnitude smaller. Spectra upstream and downstream of the 1.27-cm-thick Cu end flange are plotted in Fig. 2. The simulated spectra show the GB photon energy

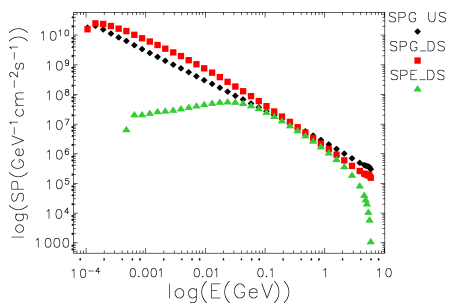

Figure 2: Spectra of photons and electrons generated by gas bremsstrahlung. The photon spectrum is given both upstream and downstream of the vacuum end flange. Electrons are only present downstream of the flange.

ranging from less than 1 MeV up to the full energy of the electron beam (in this case 6 GeV) with approximately a $1/E$ distribution where E is the photon energy; this is the case for

* Work supported by the U.S. Department of Energy, Office of Science, Office of Basic Energy Sciences, under Contract No. DE-AC02-06CH11357.
† dooling@anl.gov

ISBN: 978-3-95450-214-1 ISSN: 2673-5490 doi:10.18429/JACoW-IPAC2021-MOPAB044

unimpeded GB photons. The photon spectrum downstream of the flange shows an increase at low energies and reduction at high energies.

EXPERIMENTAL SETUP

A single element of a Pb:Glass calorimeter detector [6] was employed to detect visible Čerenkov radiation generated by the GB photons streaming down the Sector 25 insertion device (ID) front end beamline. The Pb:Glass element dimensions are 63.5 mm x 63.5 mm x 350 mm; the radiation length is 26 mm. An image of the Pb:Glass calorimeter detector is presented in Fig. 3. The walls of the Pb:Glass were

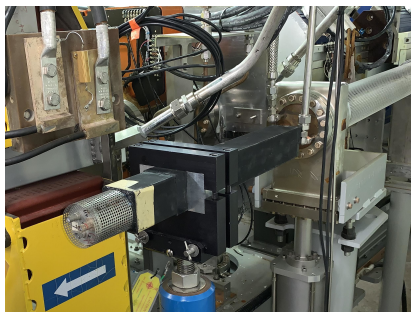

Figure 3: Pb:Glass calorimeter detector mounted in the ID25 beam line.

covered with an internally reflective, externally opaque layer. The detector senses the GB radiation when a high-energy photon enters the glass and generates an electron-positron pair. The pair produce Čerenkov light and more photons which generate more pairs leading to a pulse of light detectable by a photomultiplier tube (PMT) at the downstream end of the Pb:Glass.

We used an ITech Libera Beam Loss Monitor (BLM) field-programmable gate array (FPGA) to record signals from the PMT. The BLM FPGA allows for counting as well as single- and multi-channel pulse-height analyzer (PHA) functions. The output signal from the PMT was split twice to fill all four channels of the BLM FPGA. A schematic of the Pb:Glass detector and circuit is shown in Fig. 4.

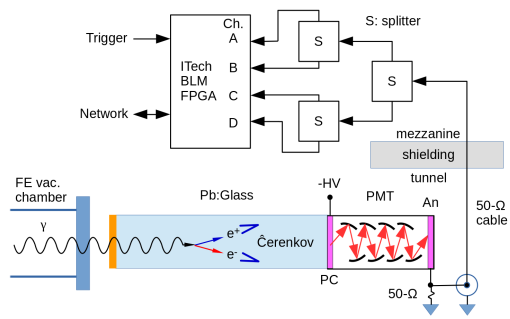

Figure 4: Pb:Glass detector and circuit schematic.

Access to the Libera BLM settings and data paths is provided by the instrument's measurement and control interface (MCI). The Libera BLM also includes a user-configurable EPICS IOC, which allows the user to access the MCI nodes using EPICS process variables. All instrument configuration and data collection is possible using standard EPICS channel access tools, including an EDM graphical user interface.

During operations, the PMT HV bias was maintained at -1.55 kV; for the gas injection study, the bias was lowered to -1.24 kV. PMT output current varies as $I_o(V) = I_{ref}(V/V_{ref})^{n-1}$, where $n = 14$ is the number of PMT dynodes. Thus gain was reduced by a factor of 18.2 during the gas injection study.

RESULTS

One of the first tasks when examining the GB data is to identify the peak energy in the spectrum. Beam energy is 7 GeV during user operations and 6 GeV during gas injection studies. By varying the threshold values of each of the four channels in separate ranges, the BLM FPGA can serve as a 4-channel PHA scanning four different energy bands simultaneously. In earlier measurements conducted in the Diagnostic ID beamline hutch, outside the SR tunnel, the maximum energy was clearly identified [7]. A reconstructed spectrum from these studies is presented in Fig. 5. Data

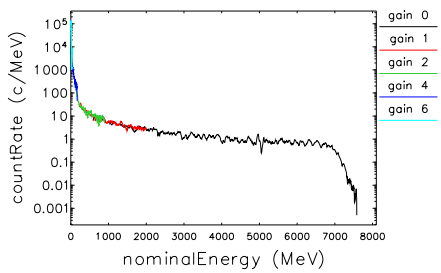

Figure 5: Earlier reconstructed GB spectrum recorded in the Diagnostic ID beamline hutch.

from separate scans are combined to produce the single spectrum shown. Of note are the non-zero count-rate data above 7 GeV; this is most likely due to a temporal pile-up of multiple lower-energy pulses [8].

Operations

We were not able to observe the upper energy limit in the acquired data sets as the threshold levels were scanned. An example of threshold scan data obtained during user operations is shown in Fig. 6; in this case, the machine was operating in 324-bunch, non-top-up mode. The count rate is normalized by beam current in mA and pressure in nTorr; the pressure is recorded in by CC1, a cold-cathode gauge installed in S25 for the gas injection experiment. The maximum ADC level in the BLM FPGA is 8191; the ADC level is equivalent to photon energy once the value corresponding to maximum photon energy is known. For the scan data plotted in Fig. 6, threshold levels were varied in ADC steps of 10, from 10 to 150 for Ch. A, 160 to 300 for Ch. B, 310 to 450 for Ch. C, and 460 to 600 for Ch. D. Due to

ISBN: 978-3-95450-214-1 ISSN: 2673-5490 doi:10.18429/JACoW-IPAC2021-MOPAB044

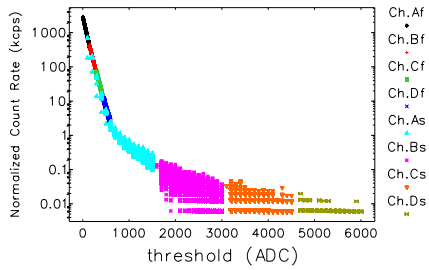

Figure 6: Threshold scans during 324-bunch, non-top-up user operations. The count rate is normalized by the beam current in mA and pressure in nTorr.

the relatively low thresholds, these channels exhibited high count rates and were sampled 100 times at each ADC value; this is termed a "fast scan." A separate scan was conducted at higher threshold levels; in this case, the levels were varied in steps of 100: from 100 to 1500 for Ch. A, 1600 to 3000 for Ch. B, 3100 to 4500 for Ch. C, and 4600 to 6000 for Ch. D. Because of the lower count rates in these threshold ranges, data was sampled 1000 times at each ADC level; this is called a "slow scan" and is also given in Fig. 6.

Threshold scans were conducted during the three operational fill patterns employed for users at the APS: 24-bunch, hybrid, and 324-bunch modes. A comparison of fast scan data at the three different fill patterns is presented in Fig. 7. The hybrid fill pattern clearly shows the largest GB signal

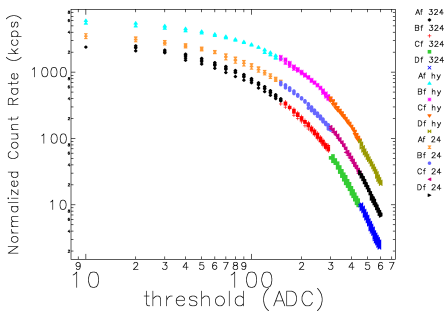

Figure 7: Comparison of fast threshold scans during 324, 24, and hybrid mode user operations. A representative cold cathode gauge gave average pressure readings of 1.68, 2.0, and 1.8 nTorr, respectively.

followed by 24-bunch and 324-bunch non-top-up modes; however, the largest pressure recorded by CC1 was during 24-bunch mode.

Gas Injection Study

For gas injection studies, the pressure in a limited length of Sector 25 straight section was raised from background to 900 nTorr, N_2 (as a worst-case scenario for radiation safety, the assumption of 1000 nT in 500 cm was used for the simulations mentioned earlier). The full pressure bump was restricted to a section of just a few meters due to pumping upstream and downstream of the leak location.

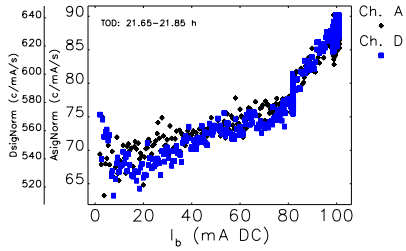

Figure 8: Normalized count rates recorded on Chs. A and D during a current transient. The normalized rates increase by 20% as the current is raised from 60 to 100 mA.

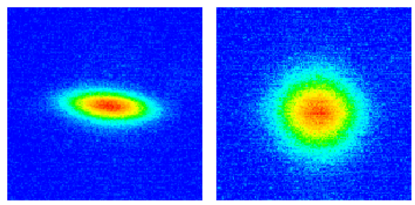

Figure 9: S35 pinhole emittance images; left: normal beam spot and right: vertical blow-up.

Normalized count rates recorded during a current transient from 0-100 mA with 900 nTorr at fixed threholds levels are presented in Fig. 8. During this time, pressure recorded by CC1 remained at 900 nTorr. The increase in count rate occurs at approximately the same time as the ion instability from trapped ions is observed in the S35 pinhole emittance camera. Vertical beam size blow up caused by trapped ions is shown in Fig. 9.

DISCUSSION AND SUMMARY

Earlier measurements with the same GB calorimeter element made in the S35 ID beamline hutch outside the tunnel [7] were able to clearly distinguish the maximum energy. Note in Fig. 3 that no shielding exists around the detector. One explanation is the background rate of high-energy shower components in the tunnel adds noise to the count rate and so the detector is not responding accurately to conditions in the straight section. Work is underway to move the detector back to a hutch outside the tunnel.

Normalized count rate differences were observed for three user beam fill patterns with the highest rates seen for hybrid mode; however, pressure measured at the gas injection location did not follow the variation. The difference may indicate variation in gas composition or additional scattering from from hybrid fill bunch pattern adding noise to the results. Regarding the gas injection study, normalized count rates show increases that correlate with observations of ion instability due to trapped ions.

ACKNOWLEDGMENTS

Thanks to M. Erdmann and R. Blake for shielding and diagnostic installation. Thanks also to R. Soliday and H. Shang for assistance with analysis scripts.

ISBN: 978-3-95450-214-1 ISSN: 2673-5490 doi:10.18429/JACoW-IPAC2021-MOPAB044

REFERENCES

[1] J. Calvey and M. Borland, "Modeling ion effects for the Argonne Advanced Photon Source upgrade," *Phys. Rev. Accel. Beams*, vol. 22, p. 114403, Nov. 2019. doi.org/10.1103/PhysRevAccelBeams.22.114403

[2] J. Calvey *et al.* "Advances in Understanding of Ion Effects in Electron Storage Rings," presented at IPAC'21, Campinas, Brazil, May 2021, paper TUXA01, this conference.

[3] W. R. Nelson, "Properties of the EM Cascade," SLAC-PUB-4203, California, USA, Feb. 1987. https://www.osti.gov/biblio/7070829

[4] Atomic and nuclear properties of air, https://pdg.lbl.gov/2015/AtomicNuclearProperties/HTML/air_dry_1_atm.html

[5] N. V. Mokhov and S. I. Striganov, "MARS15 Overview", in *AIP Conf. Proc.*, vol. 896, Mar. 2007, p. 50. doi.org/10.1063/1.2720456

[6] M. Pisharody, P.K. Job, S. Magill, J. Proudfoot, and R. Stanek, "Measurement of gas bremsstrahlung from electron storage rings", *Nucl. Instr. and Meth. in Phys. Res. A*, vol. 401, pp. 442-462, 1997. doi:10.1016/s0168-9002(97)01035-8

[7] B. Yang, private communication, January 2011.

[8] S. Usman and A. Patil, "Radiation detector deadtime and pile up: A review of the status ofscience," *Nuclear Engineering and Technology*, vol. 50, pp. 1007-1016, 2018. doi.org/10.1016/j.net.2018.06.014